

Enhanced Sparse Model for Blind Deblurring

Liang Chen¹, Faming Fang¹ *, Shen Lei², Fang Li³, and Guixu Zhang¹

¹ Shanghai Key Laboratory of Multidimensional Information Processing,
School of Computer Science and Technology, East China Normal University

² School of Software Engineering, East China Normal University

³ School of Mathematical Sciences, East China Normal University
`{liangchen527}@gmail.com, {fmfang}@cs.ecnu.edu.cn`

Abstract. Existing arts have shown promising efforts to deal with the blind deblurring task. However, most of the recent works assume the additive noise involved in the blurring process to be simple-distributed (i.e. Gaussian or Laplacian), while the real-world case is proved to be much more complicated. In this paper, we develop a new term to better fit the complex natural noise. Specifically, we use a combination of a dense function (i.e. l_2) and a newly designed enhanced sparse model termed as l_e , which is developed from two sparse models (i.e. l_1 and l_0), to fulfill the task. Moreover, we further suggest using l_e to regularize image gradients. Compared to the widely-adopted l_0 sparse term, l_e can penalize more insignificant image details (Fig. 1). Based on the half-quadratic splitting method, we provide an effective scheme to optimize the overall formulation. Comprehensive evaluations on public datasets and real-world images demonstrate the superiority of the proposed method against state-of-the-art methods in terms of both speed and accuracy.

Keywords: Blind deblurring, Noise model, Enhanced sparse model

1 Introduction

Assuming the image is degraded by a spatially-invariant blur kernel, the blurry image y can be obtained by convolving a sharp image x and a blur kernel k :

$$y = x * k + n, \quad (1)$$

where n denote the unavoidable noise. We use $*$ to represent the convolution operator. In the blind deblurring task, we aim to estimate x and k with only y . In order to solve the highly ill-posed problem, effective priors must be imposed to regularize the solution space:

$$\{x, k\} = \operatorname{argmin}_{x, k} F(y - x * k) + R_1(x) + R_2(k), \quad (2)$$

where the fidelity term $F(\cdot)$ is used to model the noise n in (1); $R_1(\cdot)$ and $R_2(\cdot)$ are used as regularization terms for x and k . It can be observed that

* Corresponding Author

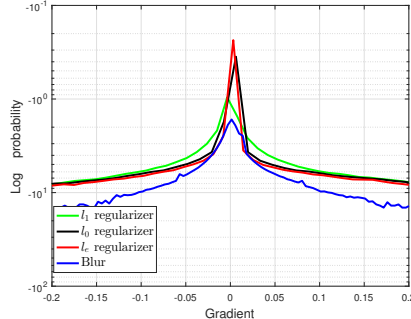


Fig. 1. Average gradient distribution of blurred images and intermediate latent images obtained from different sparse regularizers. We use the imageset from Köhler et al. [12]. The proposed l_e model shows stronger sparsity than others.

the deblurring result can benefit from a decent noise modeling step. In fact, the inappropriate noise modeling step is proved to be a major cause of the ringing artifacts appeared in the recovered image [25]. Most of former maximum a posterior (MAP)-based methods [1, 3, 13, 20, 23, 24, 28] assume the noise to follow the Gaussian or Laplacian distribution. As a result, they adopt l_2 or l_1 norm on the basic fidelity term. However, previous study has demonstrated that the noise model in natural images should be much more complex [32], assuming the distribution of noise either to follow Gaussian or Laplacian is far from convincing. Thus, in order to recover sharper images, a more reasonable noise model is required.

Inspired by the success in previous work [6] that combines a dense and a sparse model (i.e. l_2 and l_1) to model unknown noise, we conjecture if it helps to replace the l_1 model with an enhanced one. Presumably, the combination with the enhanced sparse model should be able to meet wider range of distributions, thus can better fit the complex natural noise.

To this end, we design an enhanced sparse model termed as l_e , which is based on a simple combination of the l_1 and l_0 sparse models. Surprisingly, a simple combination of these two models turns out to be sparser than either single one in practice as shown in Fig. 1, which plots the statics of the gradients of the intermediate latent images obtained by different regularizers. We observe that using the l_e model helps obtain more small gradients than that of l_0 and l_1 , which demonstrates the sparseness of the proposed model. We further give an intuitive explanation for the reason in Section 3.1.

By combining the l_e and l_2 models and considering the spatial randomness of natural noise [25], we can develop a new noise fitting function (please refer to section 3.2 for detailed description). As shown in Fig. 2, we note that the proposed noise fitting term performs more effectively than other models, and the corresponding results contain fewer artifacts as illustrated in the red boxes.

Revisiting the regularization term for the latent image. Recall that sparse priors are often adopted to penalize fine details [29] which are proved to be harmful to the deblurring process [28]. In this work, we use the proposed en-

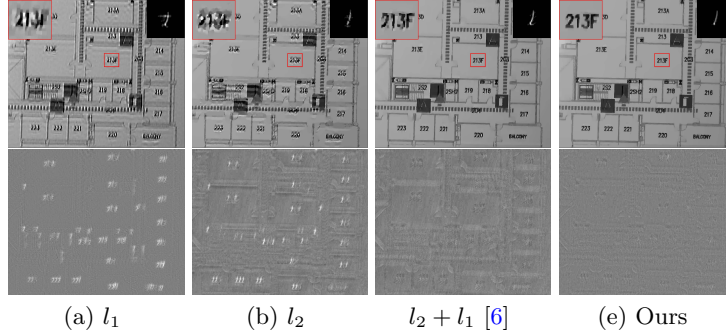


Fig. 2. Comparison between existing noise modeling strategies. The first and second row show intermediate results and corresponding noise maps from different models. Our noise map contains fewer image structures, which leads to better deblurring results.

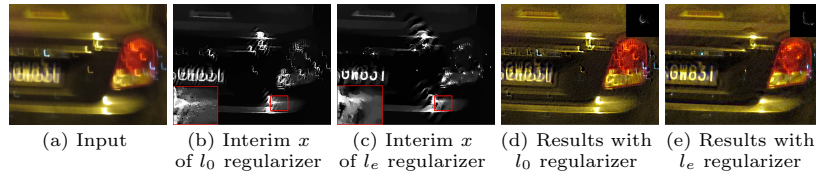


Fig. 3. Deblurring results with l_0 regularizer and l_e regularizer on latent image. The part enclosed in the red box from (b) contain insignificant pixels.

hanced sparse model to regularize the image. Besides the statistical illustration given in Fig. 1, we provide an example in Fig. 3, which shows that l_e model is able to prune more insignificant pixels than that of l_0 , and the method based on l_e also generates a better result.

Optimizing the overall non-convex formulation is challenging. We address the problem by adopting an effective half-quadratic splitting method. The whole framework is carried out in a MAP-based coarser-to-fine [3] manner. The following analysis illustrates the convergence of our model.

Contributions of this work are three-fold. (1) We propose a novel term to better fit the unknown natural noise in the blurring process. Specifically, we take advantage of a dense model (i.e. l_2) and a newly designed enhanced sparse model (i.e. l_e) to fulfill the task, in which l_e is developed from two sparse functions (i.e. l_1 and l_0). (2) We further propose to use l_e to regularize image gradients. With an unnatural representation approach [29], l_e can better penalize insignificant edges than other models. (3) Through experimental results on the benchmark datasets [12,14,16] and real-world images demonstrate that our method performs favorably against state-of-the-art methods both quantitatively and qualitatively.

2 Related Work

Previous studies demonstrate that imposing sparsity on the image gradient helps recover blurry images [4, 29]. To better achieve sparsity, some methods use spe-

cially designed regularizers to promote sparsity. Shan et al. [25] use an l_1 norm on image gradient, and incorporate it with a ringing removal term. Krishnan et al. [13] adopt a special l_1/l_2 regularization to model sparse constraint. Furthermore, Xu et al. [29] propose an unnatural l_0 sparse regularization on image gradients, and solve it in an approximation manner. Besides the sparsity of images, other statistic priors are also developed to solve the problem. For example, Pan et al. [23] introduce the dark channel prior to deblur natural images. Yan et al. [30] further propose a combination of dark channel and the opposite bright channel to improve the performance. Li et al. [18] learned a discriminative prior for the task, and Chen et al. [1] develop a local maximum gradient prior to reveal more information hidden in the blurry images.

Instead of exploring the statistical distribution of natural images, some methods select salient edges for kernel estimation. Specifically, Joshi et al. [11] extract sharp edges from blurry images by locating step edges first, and they further propagate the extrema values along the edge profile. Cho and Lee [3] adopt both bilateral and shock filtering for edge prediction. Xu and Jia [28] suggest that insignificant edges may have adverse effects on kernel estimation, and they propose a criterion for selecting informative edges. Lai et al. [14] use both filtering and data-driven prior to predict sharp edges. However, these methods will fail if there are few strong edges [23]. Thus, Gong et al. [5] propose to automatically select a subset of edges by a gradient activation method. Despite the effectiveness of these methods, they neglect the contribution of a proper noise modeling step. In this paper, we show that the proposed noise modeling strategy can boost the accuracy of the estimated kernel.

3 Proposed Method

3.1 Enhanced sparse model

The proposed enhanced sparse model is based on a combination of l_0 and l_1 sparse models given by,

$$\|\cdot\|_e = \|\cdot\|_0 + \|\cdot\|_1. \quad (3)$$

We show in the following that the l_e model can lead to a sparser solution than the widely-used unnatural l_0 approach [29] under the same condition.

Given a corrupted signal \mathcal{A} , assuming the latent signal \mathcal{B} is sparse which can be obtained by being imposed with the enhanced sparse model. With a basic quadratic penalty, the objective energy function can be expressed as following,

$$\min_{\mathcal{B}} \frac{1}{4\sigma^2} \|\mathcal{A} - \mathcal{B}\|_2^2 + \|\mathcal{B}\|_e, \quad (4)$$

where σ is the regularization parameter. Decomposing the above formulation into a set of independent sub-problems, we can rewrite (4) into,

$$\min_{\mathcal{B}_i} \frac{1}{4\sigma^2} \sum_i |\mathcal{A}_i - \mathcal{B}_i|^2 + |\mathcal{B}_i|^e, \quad (5)$$

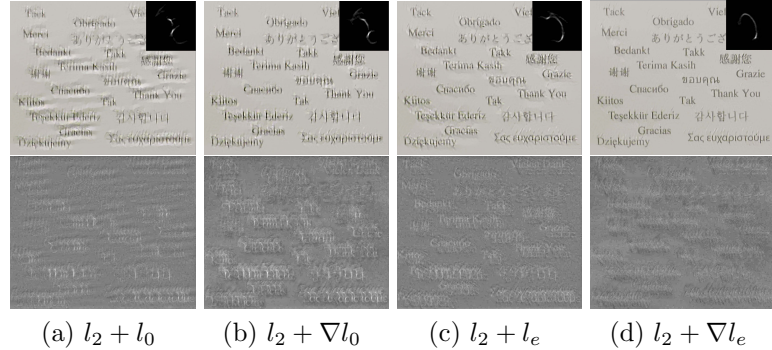


Fig. 4. Example with possible combinations of noise-fitting functions. First and second rows present deblurring results and corresponding noise maps of each noise modeling strategies. The model with $l_2 + \nabla l_e$ (i.e. proposed) generates better results and the corresponding noise map contain fewer image structure.

where i denotes the location of an element. The equation above has a closed form solution,

$$\mathcal{B}_i = \begin{cases} \mathcal{A}_i + 2\sigma^2, & \text{if } \mathcal{A}_i + 2\sigma^2 < -2\sigma \\ \mathcal{A}_i - 2\sigma^2, & \text{if } \mathcal{A}_i - 2\sigma^2 > 2\sigma \\ 0, & \text{Otherwise.} \end{cases} \quad (6)$$

Proof can be found in our supplementary material. Note that in this case the value of the latent signal \mathcal{B} will be sparser (i.e. more likely to be 0 under the same conditions) compared to the case when minimizing l_0 norm (see our supplementary file for detailed illustration), which explains the reason why l_e model is more effective at penalizing fine details. We provide further evaluation of these two models in Section 6.1.

3.2 Improved noise modeling

Instead of adopting complicate noise modeling skills, such as the mixture of Gaussian [19] or continuous mixed p norm [10], we suggest a simple combination of the l_2 norm and the enhanced sparse model to fit natural noise distribution. Empirically, our model can fit any continuous distribution in between. The noise modeling step can be written as follow,

$$F(y - x * k) = \|y - x * k\|_2^2 + \beta \|\nabla y - \nabla x * k\|_e, \quad (7)$$

where ∇ is the derivate operator in vertical and horizontal dimensions (i.e. $\nabla = \{\nabla_h, \nabla_v\}$). For simplicity, we use one order derivative operators to model the spatial randomness [25] of natural noise. As shown in Fig. 4, the model adopting both spatial randomness prior and l_e norm performs the best among possible combinations, with the result being more visually pleasing and the noise map containing fewer structures. Further comparisons are presented in Section 6.1.

3.3 Model and optimization

Analogous to previous works [5, 23, 29], we use an l_2 norm to encourage the smoothness of blur kernels. The overall deblurring model is given by,

$$\min_{x,k} \|y - x * k\|_2^2 + \beta \|\nabla y - \nabla x * k\|_e + \theta \|\nabla x\|_e + \gamma \|k\|_2^2, \quad (8)$$

where β, θ and γ are weight parameters. We obtain the solution of (8) by alternatively updating x and k with the other one fixed. The sub-problems referring to x and k are given by,

$$\begin{cases} \min_x \|y - x * k\|_2^2 + \beta \|\nabla y - \nabla x * k\|_e + \theta \|\nabla x\|_e, \\ \min_k \|y - x * k\|_2^2 + \beta \|\nabla y - \nabla x * k\|_e + \gamma \|k\|_2^2. \end{cases} \quad (9)$$

$$(10)$$

Update latent image With the intrusion of l_0 in the l_e norm, (9) becomes highly non-convex. We thus use the half-quadratic splitting method for the task. Variables u and g are introduced corresponding to $\nabla(y - x * k)$ and ∇x , respectively. Thus, (9) can be transformed into,

$$\min_{x,u,g} \|y - x * k\|_2^2 + \beta \|u\|_e + \theta \|g\|_e + \lambda_1 \|u - \nabla(y - x * k)\|_2^2 + \lambda_2 \|g - \nabla x\|_2^2, \quad (11)$$

where λ_1 and λ_2 are penalty parameters. We solve (11) by updating x, u and g separately.

(1) **Solving x .** The objective function referring to x is a quadratic problem:

$$\min_x \|y - x * k\|_2^2 + \lambda_1 \|u - \nabla(y - x * k)\|_2^2 + \lambda_2 \|g - \nabla x\|_2^2. \quad (12)$$

We can use a Fast Fourier Transform (FFT) to solve the above equation [1].

(2) **Solving u .** The subproblem referring to u is given by,

$$\min_u \beta \|u\|_e + \lambda_1 \|u - \nabla(y - x * k)\|_2^2. \quad (13)$$

Referring to (6), the solution can be written as,

$$u = \begin{cases} \{s1 | s1 = \nabla(y - x * k) - \frac{\beta}{2\lambda_1}\}, s1 > \sqrt{\frac{\beta}{\lambda_1}} \\ \{s2 | s2 = \nabla(y - x * k) + \frac{\beta}{2\lambda_1}\}, s2 < -\sqrt{\frac{\beta}{\lambda_1}} \\ 0, \quad \text{Otherwise.} \end{cases} \quad (14)$$

(3) **Solving g .** With x and u fixed, we can update g by the following equation,

$$\min_g \theta \|g\|_e + \lambda_2 \|g - \nabla x\|_2^2. \quad (15)$$

The solution of (15) is analogous to that of (13), and we omit it here.

Algorithm 1: Enhanced sparse model for blur kernel estimation

Input: Blurry image y , initialized k from the coarser level.
for $iter = 1:maxiter$ **do**
 repeat
 Updating x, u and g using Eq. (12), (13) and (15), respectively;
 $\lambda_1 \leftarrow 2\lambda_1, \lambda_2 \leftarrow 2\lambda_2$.
 until x converges;
 repeat
 Updating k and p using Eq. (17) and (18); $\lambda_3 \leftarrow 2\lambda_3$.
 until k converges;
end
Output: Blur kernel k and latent image x .

Update blur kernel The objective function *w.r.t.* k also involveing non-convex optimization. We use the same strategy as (11) by introducing new variable p for $\nabla(y - x * k)$. To boost the accuracy of the estimated kernel, we use the gradient domain instead of the intensity domain [3, 17]. Thus, (10) is reformulated to,

$$\min_{k,p} \|\nabla y - \nabla x * k\|_2^2 + \beta \|p\|_e + \gamma \|k\|_2^2 + \lambda_3 \|p - \nabla(y - x * k)\|_2^2, \quad (16)$$

where λ_3 is the weight parameter. We solve (16) by splitting it into two sub-problems referring to k, p respectively. The solution can be obtained by alternatively updating following formulations,

$$\begin{cases} \min_k \|\nabla y - \nabla x * k\|_2^2 + \lambda_3 \|p - \nabla(y - x * k)\|_2^2 + \gamma \|k\|_2^2, \\ \min_p \beta \|p\|_e + \lambda_3 \|p - \nabla(y - x * k)\|_2^2. \end{cases} \quad (17)$$

$$(18)$$

The solution of (17) can be efficiently obtained by FFT, and the problem in (18) is similar to (14). Both solutions are uncomplicated and will not be reproduced here. After obtaining k , we set the negative elements of k to 0, and normalize it to make it equal to 1. Same to existing methods, the overall kernel estimation process is implemented in a coarse-to-fine manner using an image pyramid [3]. The main steps from one pyramid level are shown in Algorithm 1.

4 Extension to Non-uniform Deblurring

The proposed model can be directly extended to non-uniform deblurring where the blur kernel across an image scale is spatially-variant. Based on the geometric model of camera motion [26, 27], the blurry image can be modeled as a weighted sum of the latent image under geometry transformations,

$$\mathbf{y} = \sum_t k_t \mathbf{h}_t \mathbf{x} + \mathbf{n}, \quad (19)$$

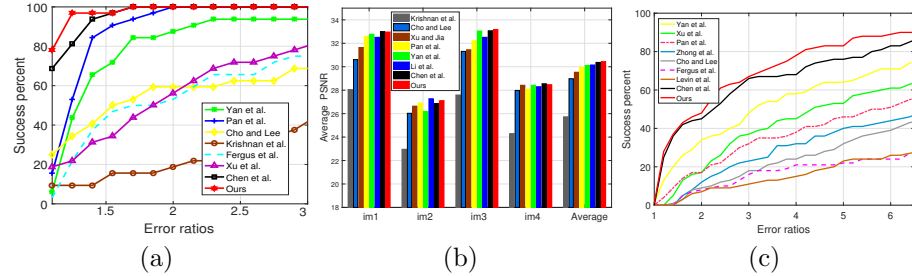


Fig. 5. Quantitative evaluations on benchmark datasets [16] [12] [15]. Our method performs competitively against existing models.

where \mathbf{y}, \mathbf{x} and \mathbf{n} denote blurry image, latent image and noise in vector form, respectively; t is the index of camera pose samples, and k_t is the corresponding weight; \mathbf{H}_t denotes a homography matrix. Similar to [27], we rewrite (19) as,

$$\mathbf{y} = \mathbf{H}\mathbf{x} + \mathbf{n} = \mathbf{z}\mathbf{k} + \mathbf{n}, \quad (20)$$

where $\mathbf{H} = \sum_t k_t \mathbf{h}_t$, $\mathbf{z} = [\mathbf{h}_1\mathbf{x}, \mathbf{h}_2\mathbf{x}, \dots, \mathbf{h}_t\mathbf{x}]$, and $\mathbf{k} = [k_1, k_2, \dots, k_t]^T$. Based on (20), the non-uniform deblurring problem is solved by alternatively minimizing,

$$\begin{cases} \min_{\mathbf{x}} \|\mathbf{H}\mathbf{x} - \mathbf{y}\|_2^2 + \beta \|\mathbf{H}\nabla\mathbf{x} - \nabla\mathbf{y}\|_e + \theta \|\nabla\mathbf{x}\|_e, \\ \min_{\mathbf{k}} \|\mathbf{z}\mathbf{k} - \mathbf{y}\|_2^2 + \beta \|\nabla\mathbf{z}\mathbf{k} - \nabla\mathbf{y}\|_e + \gamma \|\mathbf{k}\|_2^2. \end{cases} \quad (21)$$

$$(22)$$

The updating details are similar to the uniform deblurring case, and latent image \mathbf{x} and the weight \mathbf{k} are estimated by the fast forward approximation [7].

5 Experimental Results

For the hyper-parameters used in the model, we set $\beta = \theta = 0.004$ and $\gamma = 2$. We first evaluate our method on three benchmark datasets [12, 15, 16] and compare it with several state-of-the-art algorithms. Then, we examine our method on domain-specific images including text [22], face [21] and low-illumination [8] images. Similar to conventional practice, we use a non-blind deblurring method to recover final images after kernels are obtained, and we use the method from [22] unless otherwise mentioned. We implement our model in Matlab and assess the efficiency on an Intel Core i5-7400 CPU with 12GB RAM. More examples are demonstrated in our supplementary material.

5.1 Evaluation on natural images

We first evaluate our model on the dataset from Levin et al. [16] which contains 32 blurry images generated by 4 images filtered with 8 blur kernels. The images are all of size 255×255 . We compare our model with 7 generic image deblurring methods [1, 3, 4, 13, 23, 29, 30] in term of SSD error ratio [16]. As shown in Fig. 5 (a), our method performs favorably among state-of-the-art methods.

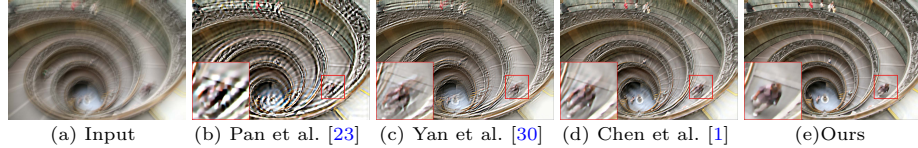


Fig. 6. A challenging example from dataset [15]. Parts enclosed in red boxes contain moderate artifacts.

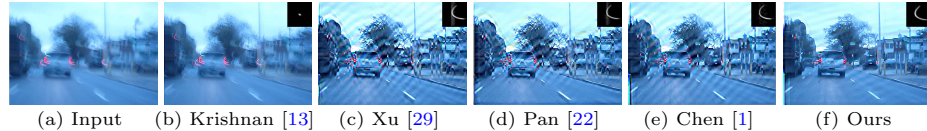


Fig. 7. Deblurring results from real-world blur images. Here we use the same non-blind deconvolution method from [2].

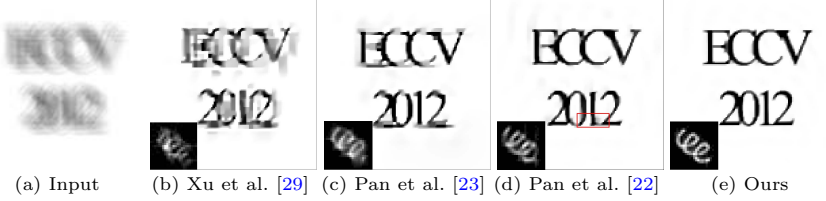
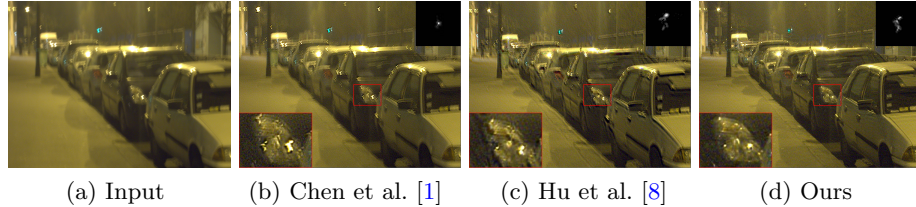
Next, we examine the proposed method on the natural image dataset from Köhler et al. [12] which contains 12 blur kernels and 4 images. We compare our result with a total of 7 recent deblurring methods [1,3,13,18,23,29,30] in term of average PSNR. We compare the PSNR values by using the protocol used in [12]. As shown in Fig. 5 (b), our method performs favorably against state-of-the-art algorithms.

We also evaluate our method on the dataset from Lai et al. [15], which contains 100 images including face, text, and low-illumination images. We compare our results to several state-of-the-art methods [1,3,4,17,22,29–31]. For fair comparison, we use the same non-blind algorithm from [2] to generate final results after acquiring blur kernels. The overall error ratios are shown in Fig. 5 (c), and our method performs the best among compared methods. A challenging example from the dataset is shown in Fig. 6, in which most state-of-the-art methods generate results with moderate ringing artifacts. In contrast, our method generates images with fewer artifacts and clearer details.

We further have our method tested in real-world blur images. In this place, we use the non-blind deconvolution method from Cho et al. [2] after obtaining the kernels of each compared method. As shown in Fig. 7, images restored by state-of-the-art methods [1,13,23,29] contain strong artifacts, while our model generates clearer edges, and is more visually pleasing.

Table 1. Results on the text dataset [22]. Our method performs favorably among existing methods.

	Cho and Lee [3]	Xu and Jia [28]	Levin et al. [17]	Xu et al. [29]	Pan et al. [23]	Li et al. [18]	Pan et al. [22]	Ours
Avg. PSNR	23.80	26.21	24.90	26.21	27.94	28.10	28.80	28.83

**Fig. 8.** Deblurring results of a text blurred image.**Fig. 9.** Deblurring results of real-world low-illumination blur image.

5.2 Evaluation on domain-specific images

Text images: We evaluate the effectiveness of our method on text blurry images by conducting experiments on the dataset provided by Pan et al. [22], which contains 15 images and 8 blur kernels from [16]. Table 1 shows the average PSNR values of each method. The proposed method performs favorably against the method specially designed for text deblurring [22]. Visually, the proposed model generated comparable results to that by [22] (Fig. 8).

Low-illumination images: As shown in Fig. 9, state-of-the-art method [1] fails to estimate the kernel due to the saturated regions. Although the method designed for low-illumination can ease the blur to some extent, their results contain residuals because the light streak is difficult to extract in this case. In contrast, our method generates results containing fewer artifacts. Note that our method is only effective with small saturated regions. Images with large saturated regions is still a challenging problem to solve.

Face images: Face blurred images are also challenging for methods that are aimed for natural images, because they often contain fewer edges or structures [21] which play a vital role in the kernel estimation process. Fig. 10 shows the final recovered results of a face blurred image by several methods. Our result has sharper edges and fewer ringing artifacts than the sate-of-the-art methods [13, 23, 29, 30].

5.3 Non-uniform deblurring

As discussed in Section 4, the proposed model can also be extended to the non-uniform deblurring task. We provide deblurring results on an image degraded by spatially-variant blur in Fig. 11. As shown in the figure, the proposed method can estimate blur kernels in every image tile and produces a comparable result with sharp edges.

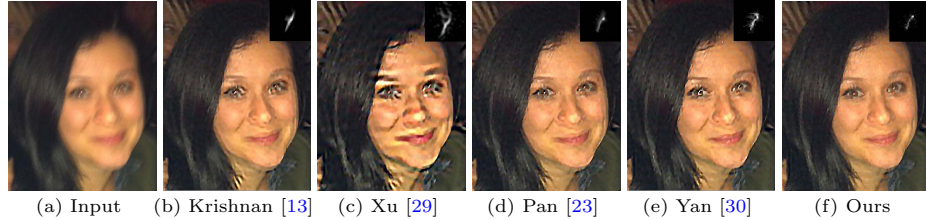


Fig. 10. Deblurring results of a real-world face blur image.

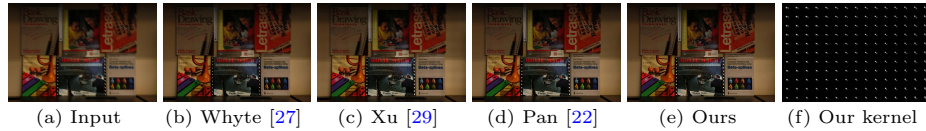


Fig. 11. Deblurring results on a non-uniform blurred image.

6 Analysis and Discussion

6.1 Effectiveness of the proposed model

The novelties of our model lie in two aspects, the l_e sparse norm and the improved noise modeling step.

We first evaluate the effectiveness of the l_e norm. We conduct ablation study on the dataset from [16]. Note in this step, the fidelity term is fixed as l_e norm while the regularization term uses different settings. As shown in Fig. 12 (a), the model with l_e imposed on regularization term is more effective than which with l_0 regularized. An example is shown in Fig. 13 (b) and (d). The proposed model with l_e (Fig. 13 (d)) generates a more visually pleasing result than that with l_0 (Fig. 13 (b)).

In (7), we impose l_2 on noise intensity domain and l_e on noise gradient (abbr. as $l_2 + \nabla l_e$) to fit natural noise while also considering its spatial randomness. We conduct ablation study on the benchmark dataset [16] to verify the effectiveness of the proposed strategy. There are a total of 6 combinations that we compare (i.e. abbr. $l_2 + \nabla l_0$, $l_2 + \nabla l_1$, $l_2 + l_e$, $l_2 + l_0$, $l_2 + l_1$ and l_2). As shown in Fig. 12 (b), the proposed setting performs the best among different combinations. Note that the noise modeling step is not as effective as others when uses only l_2 term, while with a sparse model, it performs more effectively. In another view, the performance has positive correlation with the sparsity of the sparse component (from l_1 to l_e), this phenomenon validates the rationality of our assumption. We also show that l_e on gradient domain can be more effective than that on intensity domain (black line in Fig. 12 (b)). The noise maps over iterations shown in Fig. 13 (h) and (i) also illustrate the effectiveness of the proposed noise modeling step.

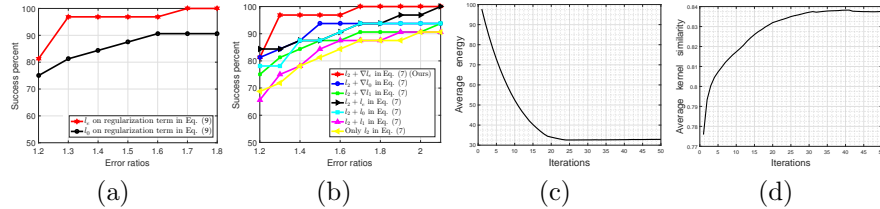


Fig. 12. (a) and (b) are ablation studies for the proposed model on the benchmark dataset [16]. (a) Effects of different sparse models for the regularization term. (b) Effects of different noise-fitting models. (c) and (d) are used to show the convergence property of the model. (c) The energy value of the objective function (9)). (d) Average kernel similarity [9].

6.2 Parameter analysis

The proposed model involves 3 main parameters, β , θ and γ . We evaluate the effects of these parameters on image deblurring in the dataset from [16] by varying one and keeping others fixed. Average PSNR is taken as an evaluation criterion. The parameter β is used to balance dense and sparse distribution in the noise model, which can benefit deblurring if it is set in a reasonable range (from 0.001 to 0.005 as shown in Fig. 14 (a)). Moreover, the best range for θ is within 0.002 to 0.008, while the value of γ has little effect on the model as shown in Fig. 14 (b) and (c).

6.3 Convergence property & running time

As our model involves non-convex regularizations, a natural question is whether our optimization scheme converges. We quantitatively evaluate the convergence property of our algorithm using the dataset [16]. We measure the values of the objective function (9), and kernel similarity [9] at finest image scale. The results are demonstrated in Fig. 12 (c) and (d), which indicates that our algorithm converges less than 50 iterations.

In addition, we test several models with different sizes of images in term of running time. The overall result is summarised in Table 2. Our method conducts one of the fastest running time among these methods.

Table 2. Running time comparisons on varying sizes of images. Codes are implemented in MATLAB unless mentioned.

	Xu (C++) [29]	Krishnan [13]	Pan [23]	Chen [1]	Ours
600 × 600	3.61	50.02	130.10	649.65	38.51
800 × 800	6.90	90.94	233.58	1680.18	70.17

6.4 Limitation

Although our method is effective in deblurring various kinds of blur images, we find its limitation in directly applying in images with large saturated areas. Fig.

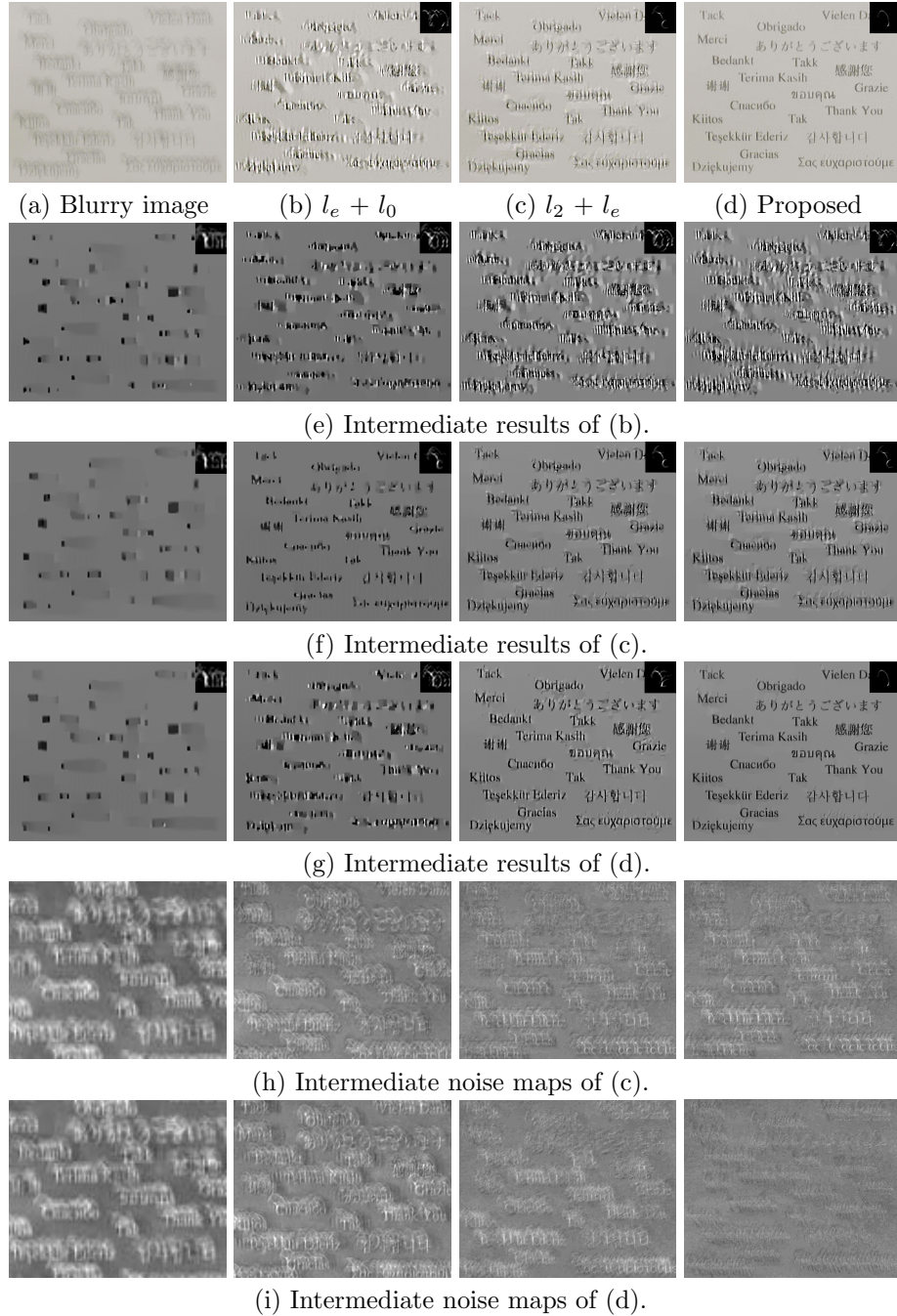
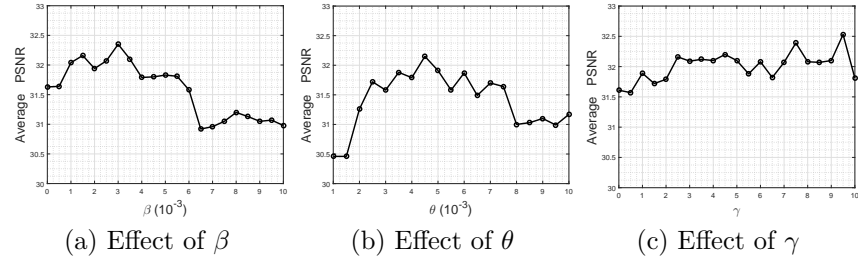
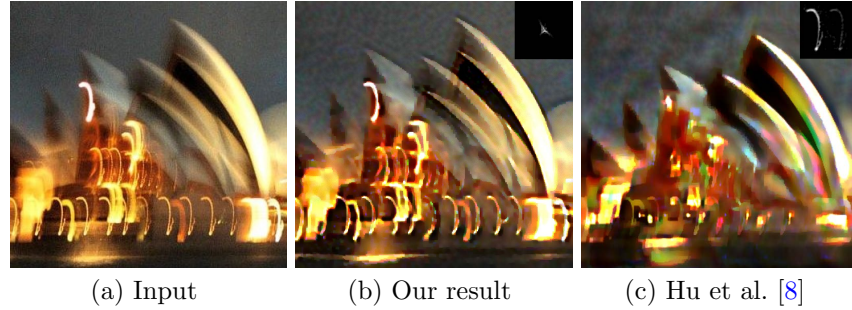


Fig. 13. Effectiveness of the proposed model. (b) Results from the proposed noise fitting model and an l_0 model to regularize image gradient. (c) Results from an l_2 model to fit noise and the proposed sparse term to regularize image gradient. The noise map using the proposed model containing fewer image structure over iterations than that without it.

**Fig. 14.** Effects of the parameters used in our model.**Fig. 15.** Limitation of the proposed model. The specially designed method [8] can handle the blurry image with large saturated regions, while our method is ineffective in this situation.

15 shows an example of deblurring image with multiple saturated regions. Our method performs poorly when directly applied in this situation, while methods designed for these tasks [8] generate a clearer result.

7 Conclusion

In this paper, we propose a new perspective for improving the blind deblurring task. In brief, we first present an enhanced sparse model, and combined it with an l_2 model to fit the complex natural noise. Then, we use the enhanced sparse model to penalize more insignificant details. To restore images regularized by the non-convex settings, we develop an effective optimization scheme based on the half-quadratic splitting method. Extensive evaluations on benchmark datasets and real-world images demonstrate that the proposed method performs favorably against state-of-the-art methods in terms of both accuracy and speed, and it works well in most given specific scenarios.

Acknowledgement This work has been sponsored by the National Natural Science Foundation of China (No. 61731009, 61871185, 61731009, and 11671002), the "Chenguang Program" supported by Shanghai Education Development Foundation and Shanghai Municipal Education Commission (17CG25), the Fundamental Research Funds for the Central Universities, and Science and Technology Commission of Shanghai Municipality (No. 19JC1420102 and 18dz2271000).

References

1. Chen, L., Fang, F., Wang, T., Zhang, G.: Blind image deblurring with local maximum gradient prior. In: CVPR (2019)
2. Cho, S., Wang, J., Lee, S.: Handling outliers in non-blind image deconvolution. In: ICCV (2011)
3. Cho, S., Lee, S.: Fast motion deblurring. ACM T. Graphics **28**(5), 145 (2009)
4. Fergus, R., Singh, B., Hertzmann, A., Roweis, S.T., Freeman, W.T.: Removing camera shake from a single photograph. ACM T. Graphics **25**(3), 787–794 (2006)
5. Gong, D., Tan, M., Zhang, Y., van den Hengel, A., Shi, Q.: Blind image deconvolution by automatic gradient activation. In: CVPR (2016)
6. Gong, Z., Shen, Z., Toh, K.C.: Image restoration with mixed or unknown noises. Multiscale Modeling & Simulation **12**(2), 458–487 (2014)
7. Hirsch, M., Schuler, C.J., Harmeling, S., Schölkopf, B.: Fast removal of non-uniform camera shake. In: ICCV (2011)
8. Hu, Z., Cho, S., Wang, J., Yang, M.H.: Deblurring low-light images with light streaks. In: CVPR (2014)
9. Hu, Z., Yang, M.H.: Good regions to deblur. In: ECCV (2012)
10. Javaheri, A., Zayyani, H., Figueiredo, M.A.T., Marvasti, F.: Robust sparse recovery in impulsive noise via continuous mixed norm. IEEE Signal Processing Lett. **25**(8), 1146–1150 (2018)
11. Joshi, N., Szeliski, R., Kriegman, D.: PSF estimation using sharp edge prediction. In: CVPR (2008)
12. Köhler, R., Hirsch, M., Mohler, B., Schölkopf, B., Harmeling, S.: Recording and playback of camera shake: Benchmarking blind deconvolution with a real-world database. In: ECCV (2012)
13. Krishnan, D., Tay, T., Fergus, R.: Blind deconvolution using a normalized sparsity measure. In: CVPR (2011)
14. Lai, W., Ding, J., Lin, Y., Chuang, Y.: Blur kernel estimation using normalized color-line priors. In: CVPR (2015)
15. Lai, W.S., Huang, J.B., Hu, Z., Ahuja, N., Yang, M.H.: A comparative study for single image blind deblurring. In: CVPR (2016)
16. Levin, A., Weiss, Y., Durand, F., Freeman, W.T.: Understanding and evaluating blind deconvolution algorithms. In: CVPR (2009)
17. Levin, A., Weiss, Y., Durand, F., Freeman, W.T.: Efficient marginal likelihood optimization in blind deconvolution. In: CVPR (2011)
18. Li, L., Pan, J., Lai, W.S., Gao, C., Sang, N., Yang, M.H.: Learning a discriminative prior for blind image deblurring. In: CVPR (2018)
19. Meng, D., la Torre, F.D.: Robust matrix factorization with unknown noise. In: ICCV (2013)
20. Michaeli, T., Irani, M.: Blind deblurring using internal patch recurrence. In: ECCV (2014)
21. Pan, J., Hu, Z., Su, Z., Yang, M.H.: Deblurring face images with exemplars. In: ECCV (2014)
22. Pan, J., Hu, Z., Su, Z., Yang, M.H.: l_0 -regularized intensity and gradient prior for deblurring text images and beyond. IEEE TPAMI **39**(2), 342–355 (2017)
23. Pan, J., Sun, D., Pfister, H., Yang, M.H.: Blind image deblurring using dark channel prior. In: CVPR (2016)
24. Ren, W., Cao, X., Pan, J., Guo, X., Zuo, W., Yang, M.H.: Image deblurring via enhanced low-rank prior. IEEE TIP **25**(7), 3426–3437 (2016)

25. Shan, Q., Jia, J., Agarwala, A.: High-quality motion deblurring from a single image. *ACM T. Graphics* **27**(3), 73 (2008)
26. Tai, Y., Tan, P., Brown, M.S.: Richardson-lucy deblurring for scenes under a projective motion path. *IEEE TPAMI* **33**(8), 1603–1618 (2011)
27. Whyte, O., Sivic, J., Zisserman, A., Ponce, J.: Non-uniform deblurring for shaken images. *IJCV* **98**(2), 168–186 (2012)
28. Xu, L., Jia, J.: Two-phase kernel estimation for robust motion deblurring. In: *ECCV* (2010)
29. Xu, L., Zheng, S., Jia, J.: Unnatural l_0 sparse representation for natural image deblurring. In: *CVPR* (2013)
30. Yan, Y., Ren, W., Guo, Y., Wang, R., Cao, X.: Image deblurring via extreme channels prior. In: *CVPR* (2017)
31. Zhong, L., Cho, S., Metaxas, D., Paris, S., Wang, J.: Handling noise in single image deblurring using directional filters. In: *CVPR* (2013)
32. Zhu, F., Chen, G., Heng, P.: From noise modeling to blind image denoising. In: *CVPR* (2016)